EFFECT OF TARTARIC ACID IN THE ELECTRODEPOSITION OF ZINC

J. Torrent-Burgués* and E. Guaus

Department of Chemical Engineering, Universitat Politècnica de Catalunya,
C/ Colom 1, 08222-Terrassa (Barcelona), Spain.
e-mail: juan.torrent @ upc.edu

Keywords: electrodeposition, nucleation model, nucleus density, sulphate bath, tartaric acid, zinc

Abstract

The electrodeposition of zinc from sulphate-tartrate baths on a vitreous carbon electrode has been studied. The influence of the tartrate ion on the reduction kinetics of Zn(II) metal ion, and on the mechanism of the electrodeposition process, has been investigated using potentiodynamic and potentiostatic electrochemical techniques and scanning electron microscopy. The voltammetric analysis has shown that the presence of tartrate species in the sulphate bath shifts the reduction potential of Zn(II) to more positive values. A set of equilibria have been proposed to represent the electrochemical process and the influence of pH. From the analysis of the chronoamperometric transients and the SEM images, an instantaneous nucleation with 2D growth at the initial stages has been proposed, and a nucleus density of the order of 10^9 cm^{-2} has been calculated from both techniques. In order to elucidate the correct mechanism of the electrodeposition process the results obtained from chronoamperometric transients must be corroborated by those of direct observation using microscopic techniques.

1. Introduction

Zinc continues to be an essential metal from a technological and industrial point of view because it is an important component in coatings and batteries. Deposits of zinc on metals, especially on steel, are extensively used to improve corrosion resistance.

Zinc electrodeposition from acid baths has been commercially practised for long time, mainly from acid chloride baths [1], but recently new studies from acid sulphate solutions have been carried out in order to obtain further insight into the dependence of the nucleation process on the electrochemical operating conditions. Although the acid sulphate bath is a known solution for zinc electrodeposition [2-4], few studies have reported the influence of complexing agents and of slightly acid pH on the nucleation process and on the deposit morphology. Thus, Raeissi et al. [5, 6] have recently studied the nucleation of electrodeposited zinc on steel in sulphate solutions at different pH values. Alvarez et al. [7] have described the nucleation and growth of zinc on HOPG in sulphate solutions in the presence of gelatine. These studies have reported the dependence of the texture and morphology of zinc electrodeposits on the nucleation and growth mechanisms and the influence of additives. Silva and Lins [8] have also studied the crystallographic texture and morphology of an electrodeposited zinc layer, varying the current density and the electrolyte flow velocity.

In this work the electrodeposition of Zn from sulphate-tartrate baths on a vitreous carbon electrode is studied mainly focusing on the influence of tartrate anions on the reduction kinetics of Zn(II) metal ions and on the mechanism of the electrodeposition process using potentiodynamic and potentiostatic electrochemical techniques. Scanning electron microscopy is used to observe the characteristics of the electrodeposits. Tartrate ion has been chosen because it is a complexing agent for the Zn(II) ion and the use of tartrate ion as organic additive in the electrodeposition of different metals and alloys has been reported [9-11].

2. Experimental

The electrochemical measurements were performed in a conventional three-electrode cell using a microcomputer-controlled AUTOLAB PSTAT 20 potentiostat/galvanostat from Eco Chemie. The chemicals used were $ZnSO_4 \cdot 7H_2O$, tartaric acid ($C_4H_6O_6$) and Na_2SO_4, all of analytical grade. All solutions were freshly prepared with water that had been twice distilled and then treated with a Millipore Milli Q system. The baths contained 1 M Na_2SO_4 as the supporting electrolyte and 0.12 M tartaric acid, as the chelating agent, the Zn(II) concentration was 0.01 M or 0.02 M and the pH was adjusted to 4 or 5 using NaOH. Before and during the experiments, which were performed at room temperature, the solutions were de-aerated with argon.

Voltammetric experiments were carried out at 50 mV s^{-1}, scanning in the negative direction. Only one cycle was run in each voltammetric experiment. Anodic stripping analysis was performed immediately after potentiostatic deposition without removing the electrode from the solution, at a scan rate of 50 mV s^{-1}.

Vitreous carbon was used as the working electrode. The vitreous carbon electrode of 0.0314 cm^2 area (Metrohm), was polished to a mirror finish before each experiment using alumina of different grades (first 3.75 and finally 1.85 μm), and cleaned ultrasonically for 2 min in water. The counter electrode was a platinum spiral. The reference electrode was an Ag/AgCl/NaCl (1 M) electrode mounted in a Luggin capillary containing Na_2SO_4 solution at the same concentration as in the bath. All potentials refer to this electrode. The morphology of the tin deposits was examined using a Jeol Cambridge L-120 scanning electron microscope.

3. Results

3.1 Voltammetric experiments

The electrochemical response of Zn(II) electrodeposition in a sulphate-tartrate bath depends on the values of total tartrate anion bulk concentration, c_L, total metallic ion Zn(II) bulk concentration, c_{Zn}, and pH, as shown in Figures 1A-1C.

Figure 1A compares the electrochemical behaviour of Zn(II) electrodeposition at pH=4 in a sulphate bath (curve a) and in two sulphate-tartrate baths (curves b and c). The concentration of sulphate, c_{SO_4}, was fixed in the three baths, and baths (b) and (c) had the same concentration of tartrate ligand, $c_{L,}$ but different Zn(II) ion concentration, c_{Zn}. In the presence of tartrate, the electrodeposition process starts at around –1.230 V, at more positive potentials than in the absence of tartrate (-1.325 V). Curve (b) shows a broad reduction peak, instead of the more well defined single peak around –1.460 V in curve (a). This broad peak corresponds to two peaks, curve (c), with a first reduction peak I_r around –1.380 V and a second reduction peak II_r around -1.580 V. In the reversed anodic scan, all three curves show a narrow oxidation peak around –1.050 V.

Figure 1B shows that an increase in pH from 4 to 5, at constant c_{SO_4}, $c_{L,}$ and c_{Zn}, produces a decrease in the intensity of the reduction peak but not in the oxidation peak. When the cathodic potential limit is –1.300 V, the characteristic nucleation loop of an electrodeposition process is obtained both at pH=4 and at pH=5 (Figure 1C).

A control cyclic voltammetric experiment was made with a blank solution containing the supporting electrolyte and the chelating agent (tartaric acid) in order to test its electrochemical response. On a vitreous carbon electrode (Figure 1D, curve a), the blank solution did not show any electrochemical response in the potential interval between 0 and –1.800 V, when the bulk hydrogen ion reduction starts. When the control experiment was repeated on a freshly prepared Zn working electrode (obtained by depositing Zn on the vitreous carbon electrode from a tartrate-sulphate bath), the blank solution exhibited a reduction wave (Figure 1D, curve b), with a peak potential around -1.465 V, very close to the previously assigned peak I_r (Figure 1D, curve c).

The efficiency of the electrodeposition process was calculated as stripping/deposition charge ratios (see Table 1), obtained from different deposition/anodic voltammetric stripping experiments (Figures 2). On one hand, the presence of tartrate ions in the bath decreases the efficiency of the process at pH=4, but does not have a significant effect at pH=5. On the other hand, at pH=4 the efficiency of electrodeposition decreases when the potential is made more negative than –1.250 V or when the c_L/c_{Zn} ratio increases.

3.2 Chronoamperometric and SEM results

Chronoamperometric curves were recorded at several potentials and in various solutions. Figure 3 shows these curves for one of the studied solutions. In order to elucidate the possible mechanism of the electrodeposition process, several analyses were carried out. The log *i* versus log *t* plots are linear, with slopes close to 1, for the initial part of the chronoamperometric curves. Figure 4 shows this behaviour for one of the studied systems, but the same is observed for the others. This slope value corresponds to instantaneous nucleation (IN) with 2D growth, according to equation (1) applicable at the initial transient [12, 13],

$$i = Kt \qquad K = 2\pi zFMhSNk^2 / \rho \qquad (1)$$

where M is the atomic weight of zinc and ρ is the solid density, S is the electrode area, F is the Faraday constant, z is the charge of the ion, N is the nucleus density, h is the thickness of the layer and k is a rate constant. This mechanism is also confirmed by the non dimensional plots of (i/i_m) versus (t/t_m) in Figure 5, according to equations (2a) and (2b) for instantaneous or progressive nucleation in 2D processes [13], respectively. In equations (2a) and (2b), i_m and t_m are the current and the time at the maximum in the chronoamperometric curves.

$$IN-2D \qquad \frac{i}{i_m} = \frac{t}{t_m}\exp\left(-0.5\,\frac{t^2 - t_m^2}{t_m^2}\right) \qquad (2a)$$

$$PN-2D \qquad \frac{i}{i_m} = \left(\frac{t}{t_m}\right)^2 \exp\left(-\frac{2}{3}\,\frac{t^3 - t_m^3}{t_m^3}\right) \qquad (2b)$$

Figure 5 shows a good coincidence in the initial transient between the experimental curves and the theoretical curve for an IN 2D process. The theoretical expression for t_m for an IN 2D growth process [13] is:

$$t_m = \frac{1}{\sqrt{2B}} \qquad with \quad B = \pi\left(\frac{M}{\rho}\right)^2 Nk^2 \qquad (2c)$$

where k, a rate constant, is equal to the product of the electrochemical rate constant k^o and the concentration c, $k=k^oc$. In our case, M=65.37 g mol^{-1}, ρ=7.14 g cm^{-3}, c= $1x10^{-5}$ or $2x10^{-5}$ mol cm^{-3}, and $k^o=6x10^{-3}$ cm s^{-1} [14]. Substituting these values in equation (2c) together with the experimental values of t_m, the values of N, the nucleus density, reported in Table 2 are obtained.

The electrodeposition mechanism was also tested separately using SEM images. Figure 6 shows SEM micrographs of an electrodeposit obtained at -1300 mV from solution C (see Table 2), and the corresponding non-dimensional analysis of the i-t transient is curve (2) in Figure 5C. Agreement with the initial part of the theoretical curve is total. The SEM images show a high density of crystallites, with a nearly flat hexagonal morphology. The calculated crystallite density is of $5.2x10^9$ cm^{-2}. This value agrees very well with the N value of $6.5x10^9$ cm^{-2} obtained from the chronoamperometric analysis considering an IN 2D process. On the other hand, the SEM micrographs show crystals of uniform size, as expected for instantaneous nucleation. The crystals show an average linear size of 140 nm.

4. Discussion and conclusions

The electrodeposition process of zinc in sulphate-tartrate baths takes place in a system containing a large number of components in solution (ligand anions, free metal ions and metal complexes) which can be described as a multiligand system. In such systems, the shape of the voltammetric response depends on the voltammetric lability of metal complexes [15-17] even working with an excess of bulk ligand concentration in solution.

Tartrate anion and sulphate anions are complexing ligands of Zn(II). The stability constants are $\log K_1=3.09$, $\log \beta_2=4.98$ for the tartrate anion, $\log K_1'=1.22$ for the

hydrogen tartrate anion and log $K_1^{''}$ = 2.30 for the sulphate anion [18]. Figure 7A shows the distribution of Zn-tartrate and Zn-sulphate complexes and Figure 7B the distribution of tartrate species as a function of pH. At pH values ≤ 3 $ZnSO_4$ is the predominating species in solution; at pH values between 3 and 5 the complexes $ZnSO_4$, ZnL and ZnL_2^{2-} coexist in solution, and at pH≥ 5 the ZnL_2^{2-} complex becomes the predominant species. The hydrogen tartrate anion, HL^-, is the predominant species at pH=4 whereas at pH=5 it is the tartrate anion, L^{2-}. From these equilibria, the electrochemical process can be represented by the following scheme:

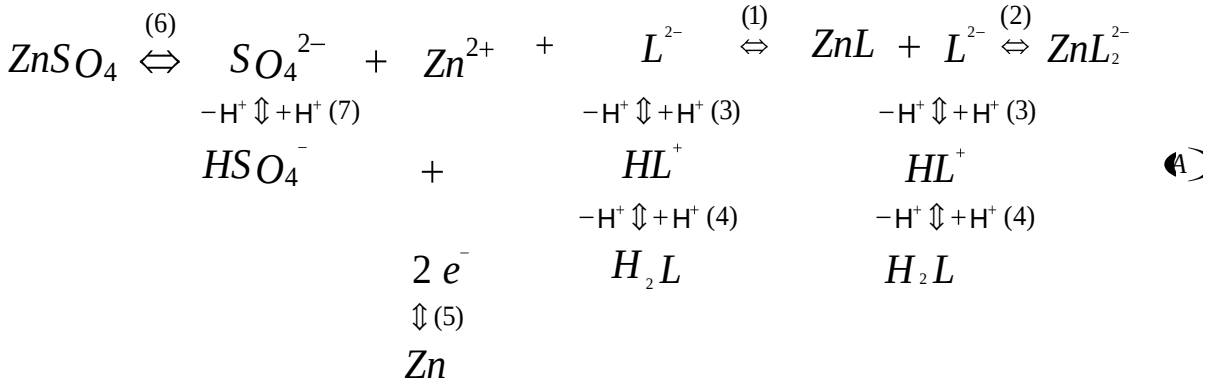

In this scheme, as is usual, it is assumed that only the Zn^{2+} is the electroactive species in solution. The possible contribution of the $ZnHL^+$ complex to the electrodeposition process has been neglected because its concentration is negligible with respect to the other Zn(II) complex species (Figure 7A).

Contrasting the scheme *A* with the voltammogram curves in Figures 1A-1D, we associate the reduction wave I_r to a reduction process via the dissociation of complexes ZnL_2^{2-} and ZnL^- (equilibria (1) and (2)), because in the presence of tartrate species in solution the electrodeposition process starts at more positive potentials (see Figure 1C) than in its absence. The loops present in Figure 1C show that at the first stages of the Zn electrodeposition process (potential limit not very negative), the current is the same at pH=4 as at pH=5. But, when the potential limit is made more negative, Figure 1B, the current at pH=4 is higher than at pH=5. We associate the increase in current with hydrogen evolution which competes with the reduction of Zn(II). The blank solution control experiment on a freshly prepared Zn electrode gives a reduction peak around -

1.465 V (Figure 1D, curve b), which is not obtained on vitreous carbon (Figure 1D, curve a). We associate this peak with the reduction of H^+ ions transported to the reaction layer by the hydrogenated tartrate ion (also by the tartaric acid depending on the pH). The discharge of H^+ ions from hydrogenated tartrate species takes place only when a Zn metallic layer has been deposited on the vitreous carbon electrode, and then the peak labelled I_r in Figures 1A and 1D, curves c, corresponds to this cathodic process. The discharge of H^+ ions from protonated organic ligand species on metallic electrodeposited layers has been described previously [19-21]. The reduction peak II_r is correlated with the reduction of the total bulk Zn(II) ion also via the dissociation of $ZnSO_4$ complex (equilibrium (6)).

Scheme *A* also explains the calculated efficiency values. Low efficiencies are associated with hydrogen evolution, as explained previously. Hydrogen evolution increases when hydrogenated tartrate species are present in solution, because H^+ ions are transported to the reaction layer by H_2L and HL^- (equilibria (3) and (4)) in order to maintain the equilibrium of formation of Zn(II) at the electrode surface. For this reason the efficiency increases with pH, i.e., when the concentration of H_2L and HL^- species in solution decreases.

Mechanisms proposed to explain electrodeposition processes depend on the experimental conditions; that is, concentration of electroactive species, potential, electrode material and preparation, pH, bath composition (additives, ligands,...). 3D growth processes are the most reported, but under certain experimental conditions, 2D growth processes have also been observed and sometimes transitions from one to another have been reported. For instance, Miranda-Hernández and González [22] reported the transition from a 3D process to a 2D for higher overpotentials in the case of silver electrodeposition in ammonium medium, and they attributed it to the growth of Ag on a previous deposited silver thin film.

Analysis of the i-t transients (Figures 4 and 5) indicates that in our case an IN 2D process occurs in the initial stage of the electrodeposition process. Nevertheless, to assure this, and due to the fact that the occurrence of a 3D process in electrodeposition has been widely reported in the literature, a non dimensional analysis accounting for a 3D growth process has also been carried out. This analysis is made according to

equations (3) [23-25] and is shown in Figure 8. The experimental curves lie in between those corresponding to instantaneous nucleation (IN) and progressive nucleation (PN), but curve (2) in Figure 8 is closer to progressive nucleation, even though it does not fit the theoretical curve perfectly, especially at the very beginning of the transient. Taking into consideration curve (2), the term AN, where A is the nucleation rate and N is the nucleus density, can be calculated using equation (4), where the parameters have the same meaning as in equation (1).

$$IN-3D \qquad \left(\frac{i}{i_m}\right)^2 = 1.95442\frac{t_m}{t}\left\{1-\exp\left[-1.2564\left(\frac{t}{t_m}\right)\right]\right\}^2 \qquad (3a)$$

$$PN-3D \qquad \left(\frac{i}{i_m}\right)^2 = 1.2254\frac{t_m}{t}\left\{1-\exp\left[-2.3367\left(\frac{t}{t_m}\right)^2\right]\right\}^2 \qquad (3b)$$

$$AN = 0.2898\left(\frac{\rho}{8\pi M}\right)^{1/2} c^{3/2}\frac{z^2F^2}{i_m^2\, t_m^3} \qquad (4)$$

The value obtained for AN is $6x10^4$ cm^{-2} s^{-1}, at -1300 mV. Considering that the usual range of values for A reported in the literature for Zn electrodeposition [7] is between 1-100 s^{-1} at moderate overpotentials, or for other metals [22, 26-28], between 1-150 s^{-1}, a value of N in the range between 10^5-10^7 cm^{-2} is obtained. This value differs from that obtained by us from SEM images, $5x10^9$ cm^{-2}, by at least two orders of magnitude. On the other hand, the uniformity in the crystal size observed by SEM (Figure 6) does not indicate a progressive nucleation event. Consequently, the occurrence of an IN 2D process in the initial part of the transient for the electrodeposition of zinc in sulphate-tartrate solutions seems justified.

The disagreement between the values of N obtained from the chronoamperometric analysis using 3D electrodeposition models and those observed by SEM, STM or AFM has been pointed out by other authors [27-29]. Brylev et al. [28] reported a 3D process with nucleation changing from progressive to instantaneous at more negative potentials, but the values of nucleus density obtained with the i-t analysis disagree with those obtained from SEM by two orders of magnitude. Gloaguen et al. [29] have also found, using STM, particle densities exceeding 10^{10} cm^{-2}, which are several orders of magnitude higher than those obtained from the analysis of i-t transients. Langerock and Heerman [27] have also found nucleus densities in the range 10^{9}-10^{10} cm^{-2} using AFM, at least three orders of magnitude higher than those obtained by fitting i-t transients. Lu and Zangari [30] also reported very high values for N (10^{9}-10^{10} cm^{-2}) observed by AFM. Thus, it seems more reasonable that the proposal of a nucleation-growth model for an experimental system from the analysis of i-t transients must be corroborated by the microscopic observation of the deposits.

As has been observed previously, different experimental conditions can lead to different mechanisms. Alvarez and Salinas [7], studying the influence of gelatine in the nucleation and growth of zinc, reported IN 3D growth in the absence of gelatine but an intermediate behaviour between IN and PN in its presence. Unfortunately these authors did not report the non-dimensional analysis for a 2D process in the initial stages, in order to discuss the applicability of this kind of mechanism in the presence of gelatine. As observed in our study, in the initial stages, a better fit to a 2D process can result. We have also observed that an IN 2D process occurs in the electrodeposition of tin in the presence of gluconate [31] under certain conditions at intermediate overpotentials.

On the other hand, as has been observed in the analysis of the current transients, the experimental curves separate from the theoretical ones at longer times, after the maximum t_m (Figure 5). This indicates that a change in the growth process occurs during electrodeposition, and that transition to a 3D growth may takes place, as also revealed by Figure 8. Due to the previous history of the process, a complete fit to neither of the pure IN or PN 3D mechanisms should apply. After the maximum, overlap of diffusion zones takes place and, at high nucleus densities, the crystal growth rate in the perpendicular direction to the surface increases relative to the parallel directions. Assuming total surface coverage, the electrodeposited charge gives a thickness *e* of 81

nm for the deposit of Figure 6. This value agrees with the thickness of 79 nm calculated from the value of N ($5.2x10^9$ cm^{-2}) and the linear crystal size value *l* of 140 nm measured in Figure 6. The fact that the ratio *e/l=0.14/0.*08 is only slightly bigger than 1 is a consequence of the high nucleus density and the occurrence of overlap. Furthermore, the Zn electrodeposits obtained in the presence of tartrate were uniform, shiny and showed fine and regular crystals, and consequently present the characteristics for a good coating.

As a final conclusion, the mismatch between nucleus densities observed by microscopic techniques and those obtained from 3D models applied to i-t transients need further investigation especially in the initial stages ($t/t_m<1$), where the possibility of 2D contributions are more likely.

Acknowledgement

This work was supported by the MCYT CTQ 2004-08046-C02-02 project (Spain).

References

1. H.H. Geduld, *Surface Cleaning, Finishing and Coating*, Metals Handbook, American Society for Metals, Ohio, 1982, vol. 5, pp. 244.
2. B.A. Lamping and T.J. O'Keefe, *Metallurg. Transact. B*, 7B (1976) 551.
3. A.R. Despic and M.G. Pavlovic, *Electrochim. Acta*, 27 (1982) 1539.
4. A.C. Beshore, B.J. Flori, G. Schade and T. J. O'Keefe, *J. Appl. Electrochem*, 17 (1987) 765.
5. K. Raeissi, A. Saatchi and M.A.Golozar, *J. Appl. Electrochem.*, 33 (2003) 635.
6. K. Raeissi, A. Saatchi, M.A.Golozar and J. A. Szpunar, *J. Appl. Electrochem.*, 34 (2004) 1249.
7. A.E. Alvarez and D.R. Salinas, *J. Electroanal. Chem.*, 566 (2004) 393.
8. J.F. Silva Filho and V.F.C. Lins, *Surf. & Coat. Tech.*, 200 (2005) 2892.

9. E. Michaillova and A. Milchev, *J. Appl. Electrochem.*, 21 (1991) 170.
10. I. A. Carlos, C. A. C. Souza, E. M. J. A Pallone, R. H. P. Francisco, J. Cardoso and B. S. Lima-Neto, *J. Appl. Electrochem.*, 30 (2000) 987.
11. Jie Cong and G. Zangari, *Mater. Sci. Eng. A*, 344 (2003) 268.
12. M. Fleischman and H.R. Thirsk, *Adv. Electrochem. & Electrochem. Eng.*, 3 (1963) 123.
13. J.A. Harrison and H.R. Thirsk, *Electroanal. Chem.*, 5 (1971) 67.
14. J.Mª Costa, *Fundamentos de electródica*, Alambra Universidad, Madrid, 1981.
15. A. Survila and P. V. Stasiukaitis, *Electrochim. Acta*, 42 (1997) 1113.
16. H. P. van Leeuwen, *Electroanalysis*, 13 (2001) 826.
17. J. Puy, J Cecilia, J Galceran, R. M. Toown and H. V. van Leeuwen, *J. Electroanal. Chem*, 571 (2004) 121.
18. Stability constants of Metal-ion Complexes, *IUPAC Chemical Data Series nº 22*. Pergamom Press, Oxford, 1979.
19. E. Guaus and J. Torrent-Burgués, *Russ. J. Electrochem.*, 42 (2006) 141.
20. J. Büdienė, A. Surviliene, A. Survila, *Russ. J. Electrochem.* 40 (2004) 394.
21. A. Survila, A. Survilienė, S. Kanapeckaitė, J. Büdienė, P. Kalinauskas, G. Stalnionis, A. Sudavičius, *J. Electroanal. Chem.* 582 (2005) 221.
22. M. Miranda-Hernández and I. González, *J. Electrochem. Soc*., 151(3) (2004) C220.
23. B.R. Scharifker and G.J. Hills, *Electrochim. Acta*, 28 (1983) 879.
24. G.A. Gunawardena, G.J. Hills, I. Montenegro and B.R. Scharifker, *J. Electroanal. Chem.*, 138 (1982) 225.
25. B.R. Scharifker and J. Mostany, *J. Electroanal. Chem.*, 177 (1984) 13.
26. K. Márquez, G. Staikov and J.W. Schultze, *Electrochim. Acta*, 48 (2003) 875.
27. S. Langerock and L. Heerman, *J. Electrochem. Soc.*, 151 (2004) C155.
28. O. Brylev, L. Roué and D. Bélanger, *J. Electroanal. Chem.*, 581 (2005) 22.
29. F. Gloaguen, J.M. Léger, C. Lamy, A. Marmann, U. Stimming and R. Vogel, *Electrochim. Acta*, 44 (1999) 1805.
30. G. Lu and G. Zangari, *Electrochim. Acta*, 51 (2006) 2531.
31. J. Torrent-Burgués, E. Guaus and F. Sanz, *J. Appl. Electrochem*., 32 (2002) 225.

Table 1. Calculated efficiencies for different experimental conditions in deposition/anodic stripping experiments (t_d: deposition time, E_d: deposition potential).

c_L/M	c_{Zn}/M	pH	t_d/s	E_d/ V	Efficiency/ %
0	0.01	4	30	-1.340	75
		5	10	-1.300	80
0.12	0.01	4	40	-1.250	56
				-1400	30
		5	40	-1250	81
				-1400	77
0.12	0.02	4	40	-1250	62
				-1.400	40

Table 2. Calculated nucleus density according to an IN 2D process

	Solution A (1)	Solution B (2)	Solution C (3)
-E / mV	N 10^{-10} / cm^{-2}	N 10^{-10} / cm^{-2}	N 10^{-10} / cm^{-2}
1275			0.20
1300		0.54	0.65
1325	0.18	0.65	1.0
1350	0.53	1.6	
1375	0.99	2.8	3.7
1425	1.8	9.5	

(1) Solution A: 0.01 M $ZnSO_4$ + 1 M Na_2SO_4 + 0.12 M $C_4H_6O_6$, at pH= 4.
(2) Solution B: 0.01 M $ZnSO_4$ + 1M Na_2SO_4 + 0.12 M $C_4H_6O_6$, at pH= 5.
(3) Solution C: 0.02 M $ZnSO_4$ + 1 M Na_2SO_4 + 0.12 M $C_4H_6O_6$, at pH= 4.

Captions for figures

Figure 1A. Cyclic voltammograms of a vitreous carbon electrode in a 0.01 M $ZnSO_4$ + 1 M Na_2SO_4 solution at pH= 4 (solid curve a), 0.01 M $ZnSO_4$ + 1M Na_2SO_4 + 0.12 M $C_4H_6O_6$ solution at pH= 4 (dotted curve b) and 0.02 M $ZnSO_4$ + 1 M Na_2SO_4 + 0.12 M $C_4H_6O_6$ solution at pH= 4 (dashed curve c). Arrows indicate scan direction. In all cases v= 50 mV s^{-1}.

Figure 1B. Cyclic voltammograms of a vitreous carbon electrode at v= 50 mV s^{-1} in a 0.01 M $ZnSO_4$ + 1 M Na_2SO_4 + 0.12 M $C_4H_6O_6$ solution and pH= 4 (solid curve a) and pH= 5 (dotted curve b). Cathodic potential limit = -1.8 V. Arrow indicates scan direction.

Figure 1C. Cyclic voltammograms of a vitreous carbon electrode at v= 50 mV s^{-1} in a 0.01 M $ZnSO_4$ + 1 M Na_2SO_4 + 0.12 M $C_4H_6O_6$ solution at pH= 4 (solid curve a) and pH= 5 (dotted curve b). Cathodic potential limit = -1.3 V. Arrow indicates scan direction.

Figure 1D. Cyclic voltammograms of a vitreous carbon electrode at v= 50 mV s^{-1} in a 1 M Na_2SO_4 + 0.12 M $C_4H_6O_6$ solution at pH= 4 (dotted curve a) and 0.01 M $ZnSO_4$ + 1 M Na_2SO_4 + 0.12 M $C_4H_6O_6$ solution at pH= 4 (dashed curve c). Cyclic voltammogram of a zinc electrode at v= 50 mV s^{-1} in a 1 M Na_2SO_4 + 0.12 M $C_4H_6O_6$ solution at pH= 4 (solid curve b). Arrow indicates scan direction.

Figure 2. Anodic stripping voltammograms of zinc deposits obtained after 40 s at -1.250 V (A) and at -1.400 V (B) on a vitreous carbon electrode in a: 0.01 M $ZnSO_4$ + 1 M Na_2SO_4 solution at pH= 4 (solid curve a), 0.01 M $ZnSO_4$ + 1M Na_2SO_4 + 0.12 M $C_4H_6O_6$ solution at pH= 4 (dotted curve b) and 0.02 M $ZnSO_4$ + 1 M Na_2SO_4 + 0.12 M $C_4H_6O_6$ solution at pH= 4 (dashed curve c). The deposited charges in Figure A are: a) 0.55 mC; b) 0.57 mC; c) 2.35 mC. The deposited charges in Figure B are: a) 2.36 mC; b) 1.55 mC; c) 3.94 mC. In all cases v= 50 mV s^{-1}

Figure 3. Chronoamperometric transients for a 0.01 M $ZnSO_4$ + 1M Na_2SO_4 + 0.12 M $C_4H_6O_6$ solution at pH= 4. Curves at E= -1325 mV (1), -1350 mV (2), -1375 mV (3) and -1425 mV (4).

Figure 4. Logarithmic analysis, log i vs log t, for the chronoamperometric curves for a 0.01 M $ZnSO_4$ + 1M Na_2SO_4 + 0.12 M $C_4H_6O_6$ solution at pH= 4, E= -1325 mV (1), -1350 mV (2), -1375 mV (3), -1425 mV (4), -1450 mV (5).

Figure 5. Non dimensional analysis (i/i_m) vs (t/t_m) of the chronoamperometric curves, A) 0.01 M $ZnSO_4$ + 1M Na_2SO_4 + 0.12 M $C_4H_6O_6$ solution at pH= 4, E= -1350 mV (1), -1375 mV (2), -1425 mV (3). B) 0.01 M $ZnSO_4$ + 1 M Na_2SO_4 + 0.12 M $C_4H_6O_6$ solution at pH= 5, E= -1300 mV (1), -1375 mV (2), -1425 mV (3). C) 0.02 M $ZnSO_4$ + 1 M Na_2SO_4 + 0.12 M $C_4H_6O_6$ solution at pH= 4, E= -1275 mV (1), -1300 mV (2), -1325 mV (3).

Figure 6. A) SEM micrograph obtained for a 0.02 M $ZnSO_4$ + 1 M Na_2SO_4 + 0.12 M $C_4H_6O_6$ solution at pH= 4, without agitation, -1300 mV and 40 s. Deposited charge density of 0.17 C cm^{-2}. B) A zoom of A. Dimension bars are at the bottom of micrographs.

Figure 7A. Concentration of Zn(II)-sulphate and Zn(II)-tartrate complexes vs pH, for a total sodium sulphate concentration of 1 M, a total bulk acid tartaric concentration of 0.12 M and a total bulk Zn(II) concentration of 0.02 M.

Figure 7B. Concentration distribution of tartrate species vs pH, for a 0.12 M total bulk concentration of tartaric acid.

Figure 8. Non dimensional analysis $(i/i_m)^2$ vs (t/t_m) of the chronoamperometric curves, for a 0.02 M $ZnSO_4$ + 1 M Na_2SO_4 + 0.12 M $C_4H_6O_6$ solution at pH= 4, E= -1275 mV (1), -1300 mV (2), -1325 mV (3).

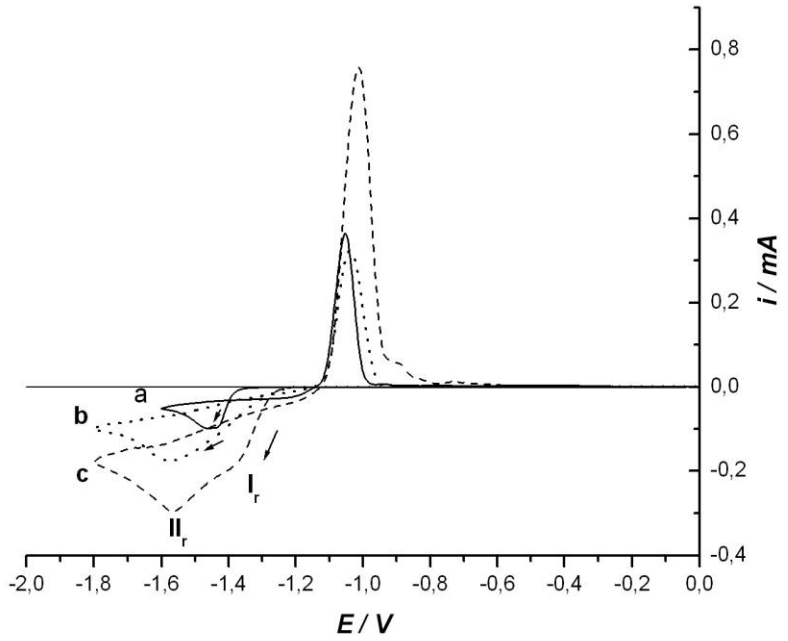
0,8
0,6
0,4
0,2
0,0
-0,2
-0,4
i / mA
a
b
c
I r
II r
-2,0 -1,8 -1,6 -1,4 -1,2 -1,0 -0,8 -0,6 -0,4 -0,2 0,0
E / V

Fig 1A

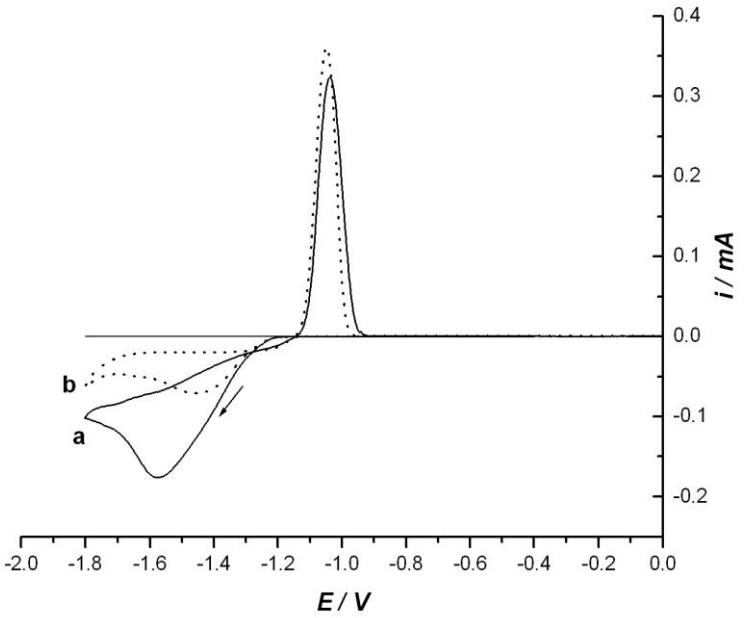
0.4
0.3
0.2
0.1
0.0
-0.1
-0.2
i / mA
b
a
-2.0 -1.8 -1.6 -1.4 -1.2 -1.0 -0.8 -0.6 -0.4 -0.2 0.0
E / V

Fig 1B

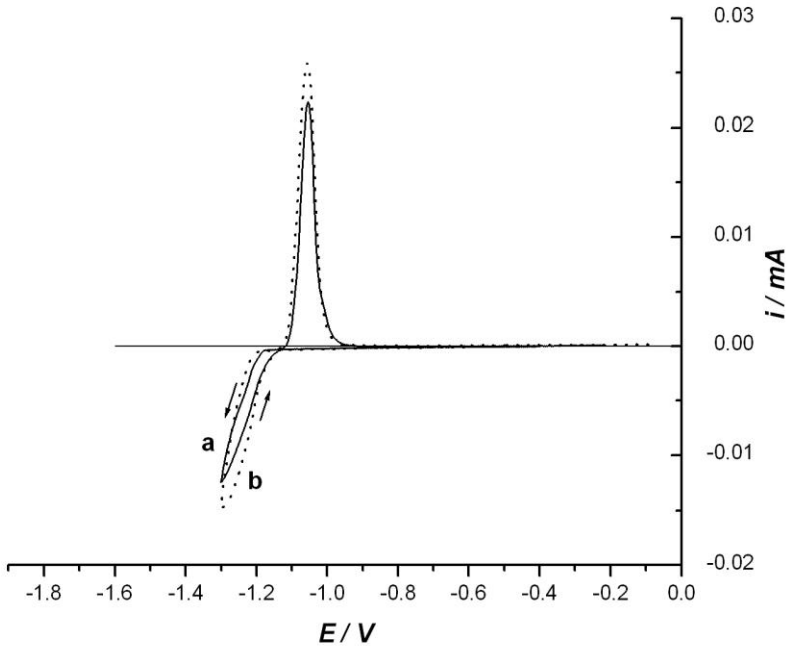
0.03
0.02
0.01
0.00
-0.01
-0.02
i / mA
a
b
-1.8
-1.6
-1.4
-1.2
-1.0
-0.8
-0.6
-0.4
-0.2
0.0
E / V

Fig 1C

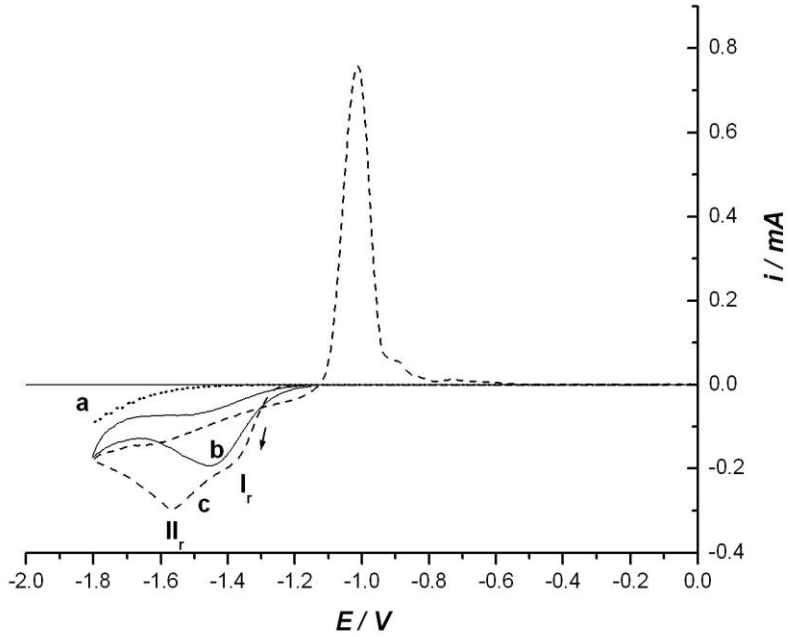
0.8
0.6
0.4
0.2
0.0
-0.2
-0.4
i / mA
a
b
c
I r
II r
-2.0
-1.8
-1.6
-1.4
-1.2
-1.0
-0.8
-0.6
-0.4
-0.2
0.0
E / V

Fig 1D

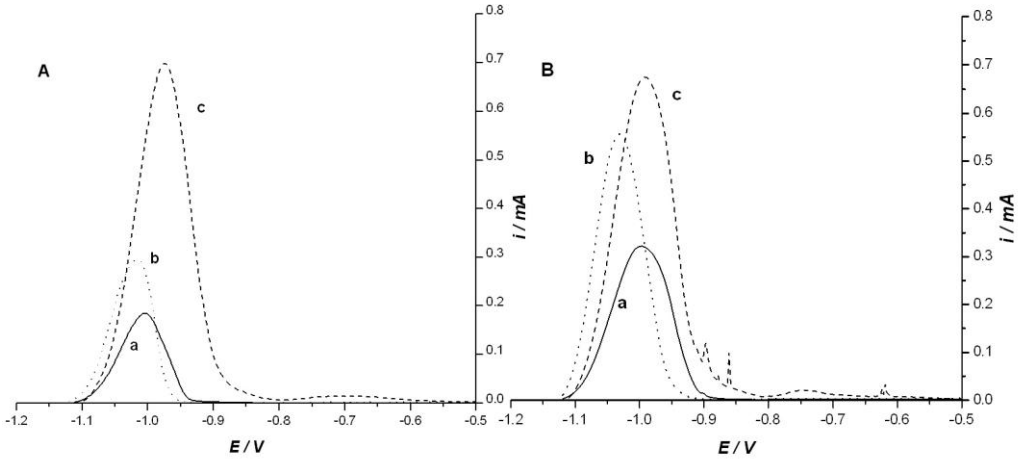

Fig 2

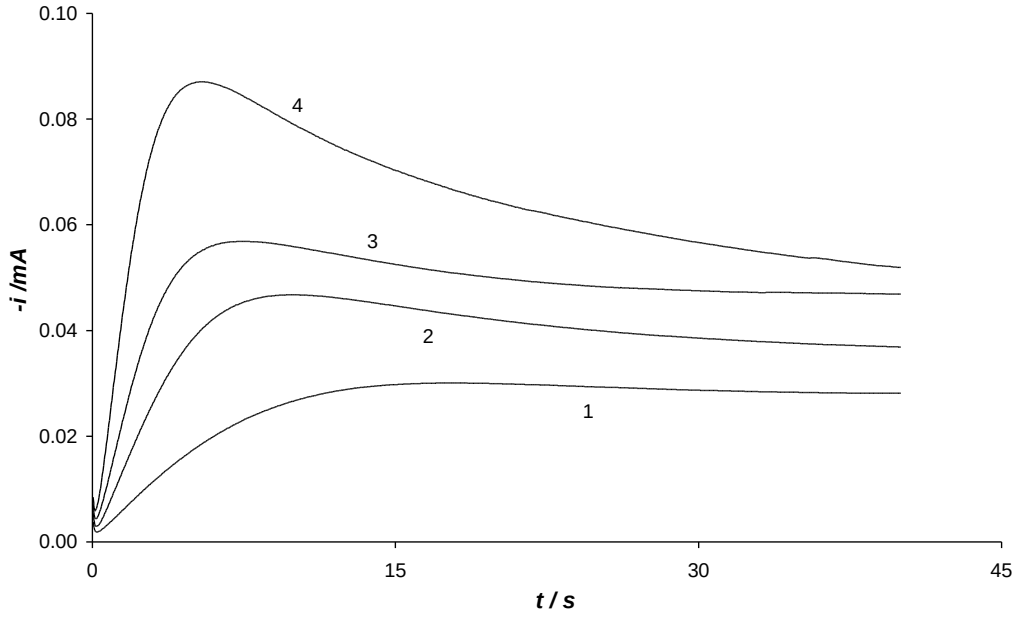

Fig 3

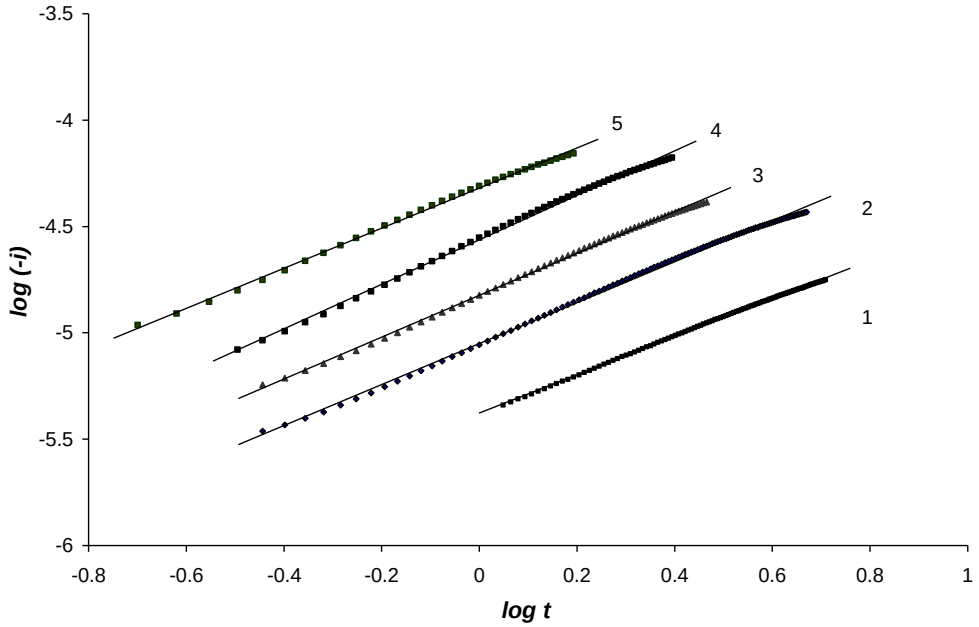
-3.5
-4
-4.5
-5
-5.5
-6
log (-i)
-0.8
-0.6
-0.4
-0.2
0
0.2
0.4
0.6
0.8
1
log t
5
4
3
2
1

Fig 4

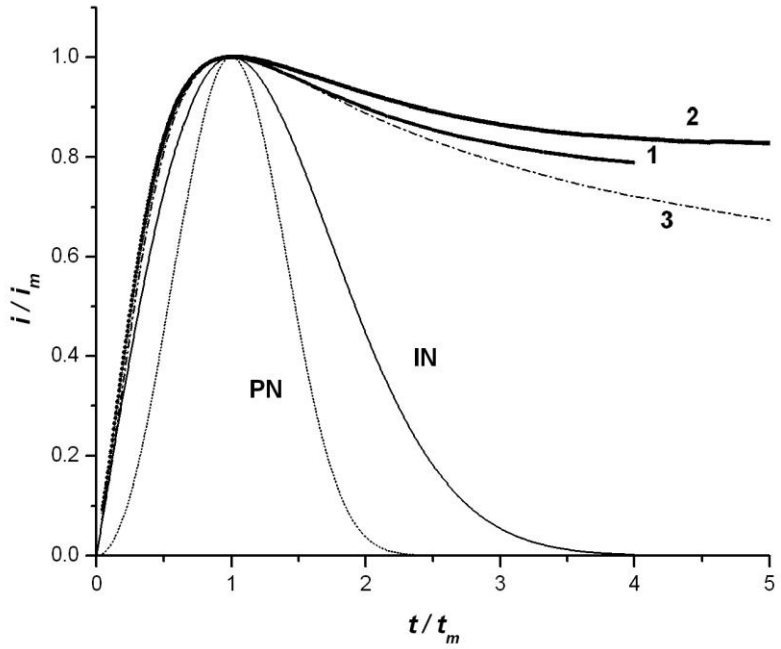
1.0
0.8
0.6
0.4
0.2
0.0
i / i_m
0
1
2
3
4
5
t / t_m
2
1
3
IN
PN

Fig 5A

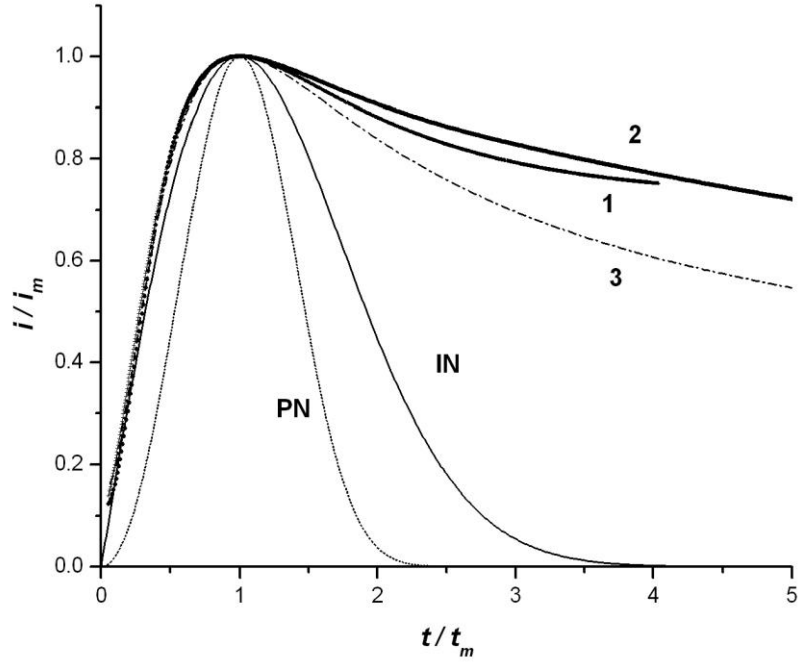
1.0
0.8
0.6
0.4
0.2
0.0
0
1
2
3
4
5
i / i_m
t / t_m
2
1
3
IN
PN

Fig 5B

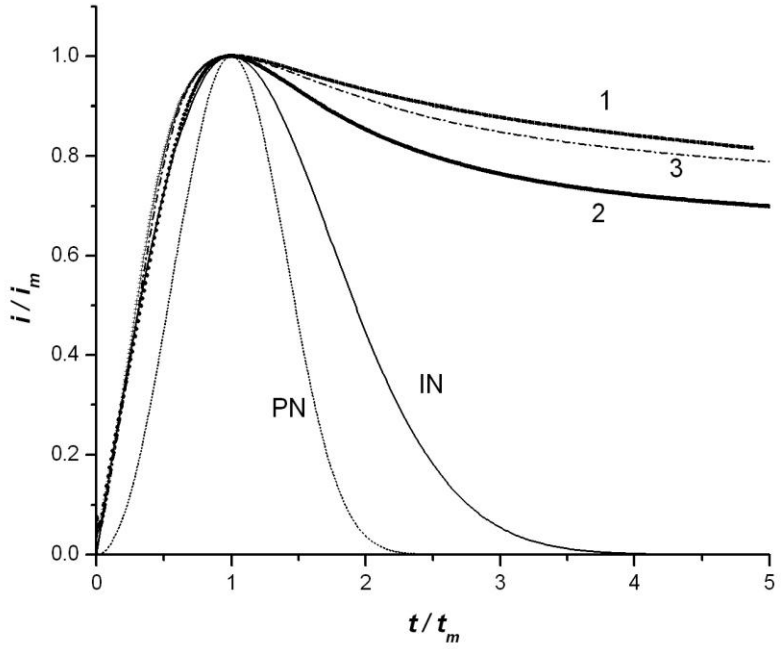
1.0
0.8
0.6
0.4
0.2
0.0
0
1
2
3
4
5
i / i_m
t / t_m
1
3
2
IN
PN

Fig 5C

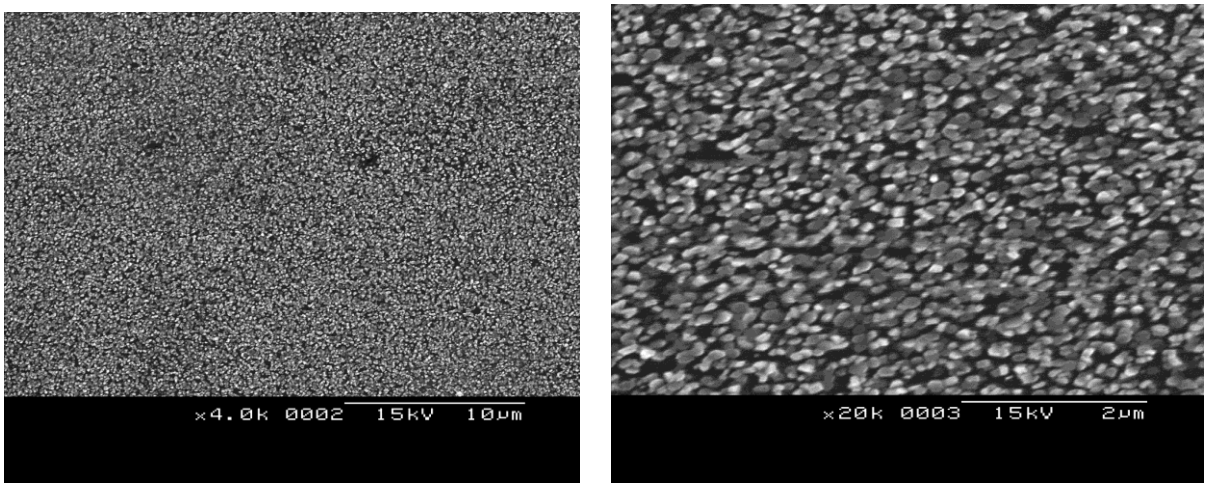

A B

Fig 6

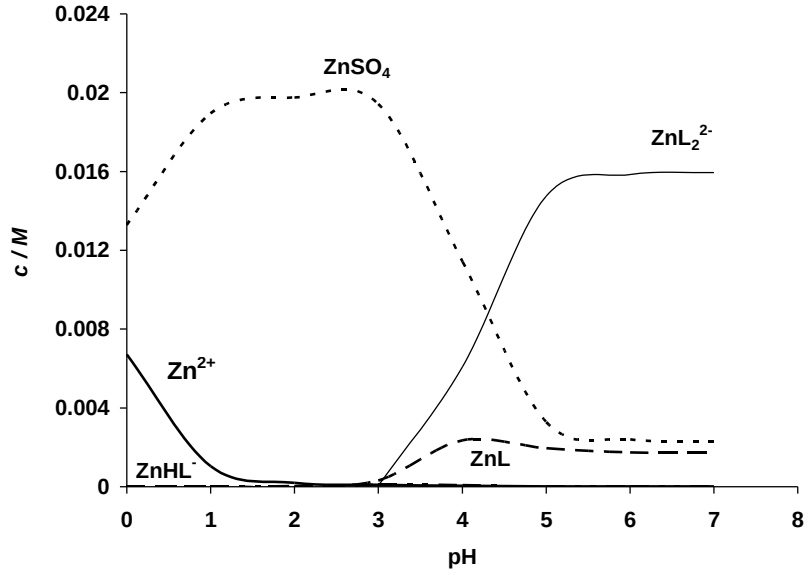

Fig 7A

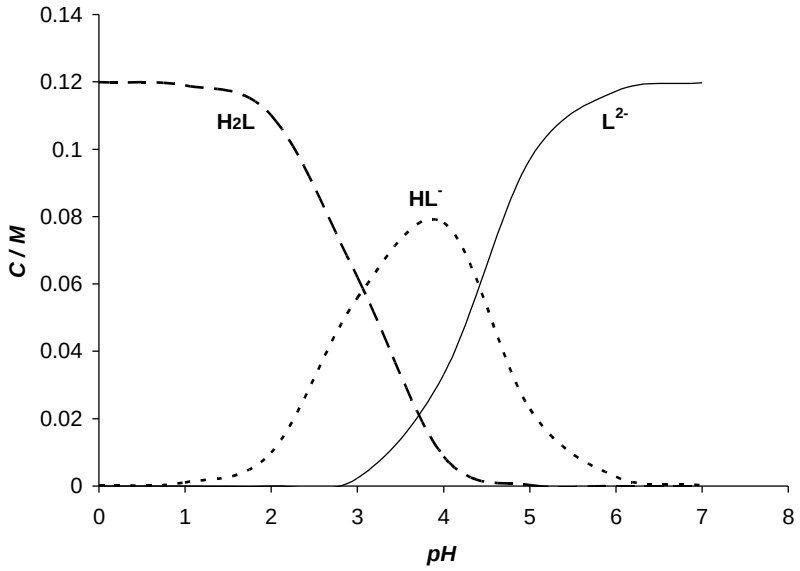
0.14
0.12
0.1
0.08
0.06
0.04
0.02
0
C / M
H2L
HL-
L2-
0
1
2
3
4
5
6
7
8
pH

Fig 7B

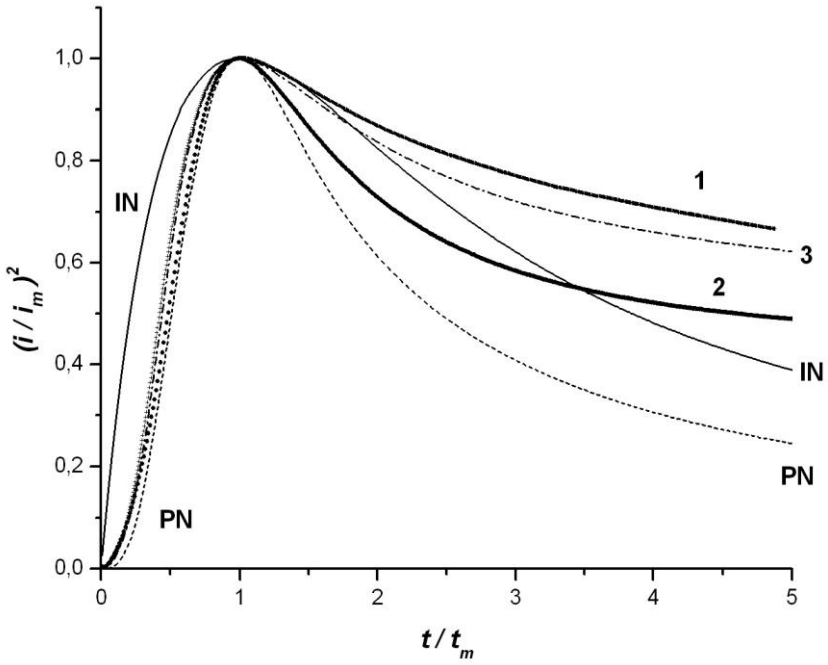
1,0
0,8
0,6
0,4
0,2
0,0
(i / im)2
IN
PN
1
3
2
IN
PN
0
1
2
3
4
5
t / tm

Fig 8